A Nonlinear Acoustic Technique for Crack Detection in Metallic Structures

Debaditya Dutta, Hoon Sohn, Kent A. Harries and Piervincenzo Rizzo

Structural Health Monitoring 2009 8: 251
DOI: 10.1177/1475921709102105

SHM
Structural Health Monitoring

A Nonlinear Acoustic Technique for Crack Detection in Metallic Structures

Debaditya Dutta,[1] Hoon Sohn,[1,2,*] Kent A. Harries[3] and Piervincenzo Rizzo[3]

[1]*Department of Civil and Environmental Engineering, Carnegie Mellon University, 5000 Forbes Avenue, Pittsburgh, PA – 15213, USA*
[2]*Department of Civil and Environmental Engineering, Korea Advanced Institute of Science and Technology, Daejeon 305-701, Korea*
[3]*Department of Civil and Environmental Engineering, University of Pittsburgh, Pittsburgh, PA – 15261, USA*

A crack detection technique based on nonlinear acoustics is investigated in this study. Acoustic waves at a chosen frequency are generated using an actuating lead zirconate titanate (PZT) transducer, and they travel through the target structure before being received by a sensing PZT wafer. Unlike an undamaged medium, a cracked medium exhibits high acoustic nonlinearity which is manifested as harmonics in the power spectrum of the received signal. Experimental results also indicate that the harmonic components increase nonlinearly in magnitude with increasing amplitude of the input signal. The proposed technique identifies the presence of cracks by looking at the two aforementioned features: harmonics and their nonlinear relationship to the input amplitude. The effectiveness of the technique has been tested on aluminum and steel specimens. The behavior of these nonlinear features as crack propagates in the steel beam has also been studied.

Keywords nondestructive testing (NDT) · active sensing · nonlinear acoustics · harmonics · fatigue cracks

1 Introduction

Metallic structures made of aluminum and steel are ubiquitous in mechanical, aerospace, and civil infrastructure. Structural failure in metals is often attributed to cracks developed due to fatigue or fracture. For instance, such cracks can develop at the flange-web junction of a bridge girder, in the wings of an aircraft, in railway tracks or in the sub-structures of a power generation plant. In most cases, cracks cannot be avoided. Thus there is a need for nondestructive inspection of such structural components.

Some of the popular NDT techniques for crack detection are acoustic emission [1], eddy current techniques [2], vibration-based techniques [3], impedance-based methods [4–6] and ultrasonic testing [7–21]. Ultrasonic testing using guided waves has recently gained popularity in those monitoring applications that can benefit from built-in transduction, moderately large inspection ranges, and high sensitivity to small flaws. Guided wave-based methods can be

*Author to whom correspondence should be addressed.
E-mail: hoonsohn@kaist.ac.kr
Figures 3–8 and 10–16 appear in color online: http://shm.sagepub.com

Vol 8(3): 0251–12
[1475-9217 (200903) 8:3;251–12 10.1177/1475921709102105]

broadly classified in two groups: (1) those based on the principles of linear acoustics like transmission, reflection, scattering, mode-conversion, and absorption of acoustic energy caused by a defect [7–12]; and (2) those based on the principles of nonlinear acoustics like harmonics generation [13–17], frequency mixing [18,19], and modulation of ultrasound by low-frequency vibration [20,21]. Linear NDT techniques identify cracks by detecting the amplitude and phase change of the response signal caused by defects when a consistent probe signal is applied. On the other hand, nonlinear techniques correlate defects with the presence of additional frequency components in the output signal. Existing literature on damage detection techniques using nonlinear acoustics [18,19] suggest that nonlinear techniques are robust to harmless factors like complicated geometry or moderate environmental variations *viz*. wind and temperature. This robustness makes the nonlinear acoustic techniques attractive for field applications.

Many existing techniques suffer from one or more drawbacks *viz*. use of bulky equipment, unsuitability of automation and requirement of interpretation of data or image by trained engineers. These shortcomings make existing methods less attractive for online continuous monitoring. The uniqueness of the present study lies in the authors' effort to overcome the aforementioned drawbacks by developing a crack detection technique using PZT wafers (which can be easily surface-mounted or embedded in the structure) and suggesting a damage detection process that can be readily automated. These features might make the proposed technique more suitable for online continuous monitoring of structures. Another unique aspect of this paper is to study the behavior of the nonlinear features with a propagating crack in a steel beam.

The paper is organized as follows. First, the theoretical development for acoustic nonlinearity due to cracks is provided. Then, experimental studies performed to verify the effectiveness of the proposed technique are discussed. Finally, this paper concludes with a brief summary.

2 Theoretical Backgrounds Behind Harmonics Generation due to Crack Formation

Fatigue in metallic materials is a progressive, localized, and permanent structural damage that occurs when a material is subjected to cyclic or fluctuating stresses that are less than (often much less than) the static yield strength of the material [22]. The process initiates a discontinuity and becomes a microscopic crack. The crack propagates as a result of subsequent stress applications caused by cyclic loading. The fatigue life depends on the applied stress range and also on the structural geometry. A higher stress range usually leads to shorter fatigue life.

It is well known that a crack in a metallic structure causes nonlinear interaction of acoustic waves [13–21]. A manifestation of this nonlinear interaction is the production of acoustic superharmonics when the structure is excited with an ultrasonic probing signal of a given frequency [13–17]. Several theories have been proposed to explain the phenomenon of harmonics generation. However, a consensus regarding the physical understanding of the mechanism has not yet been reached. A summary of the existing theoretical models has been given by Parsons and Staszewski [21]. One of the popular theories is the 'breathing crack model' where the crack closes during compression and opens during tension when ultrasonic waves propagate through it [14,16–19,23,24]. In the following paragraphs, the authors have endeavored to explain the phenomenon of harmonics generation in a semi-analytic manner. The intention is to provide an easy and intuitive understanding of the above phenomenon without indulging into a rigorous mathematical analysis. A variational formulation, similar to that of the finite element method, has been adopted for the purpose of the semi-analytic derivation. The crack is modeled as a single infinitesimal element in the structure that exhibits bilinear stiffness [14,16–19,23].

Consider a longitudinal wave traveling through a slender elastic beam containing a crack (Figure 1). The beam is fixed at one end and excited with a harmonic stress at the other. The bilinear stress–strain relationship at the location

of the crack is shown in Figure 2. As a convention, the strain (ε) is considered positive in tension and negative in compression. Mathematically, therefore, the crack is open when $\varepsilon|_{x_c} > 0$ and closed when $\varepsilon|_{x_c} < 0$.

If the mass density of the beam in question is assumed to be uniform and equal to ρ, the governing equation of wave propagation through this structure is given by:

$$\rho\frac{\partial^2 u}{\partial t^2} = \frac{\partial}{\partial x}\left(E\frac{\partial u}{\partial x}\right)$$
$$E = \begin{cases} E_2 & \text{for } x = x_c \text{ and } \varepsilon|_{x=x_c} = \left.\dfrac{\partial u}{\partial x}\right|_{x=x_c} > 0 \\ E_1 & \text{otherwise} \end{cases} \tag{1a}$$

where $u = u(x, t)$ is the longitudinal displacement of a point on the beam at position x and time t, and $E = E(x, \partial u/\partial x)$ is the modulus of elasticity.

Equation 1a is subject to the initial conditions:

$$\begin{aligned} u|_{t=0} &= 0 \quad \text{for } 0 \le x \le L \\ \left.\frac{\partial u}{\partial t}\right|_{t=0} &= 0 \quad \text{for } 0 \le x \le L \end{aligned} \tag{1b}$$

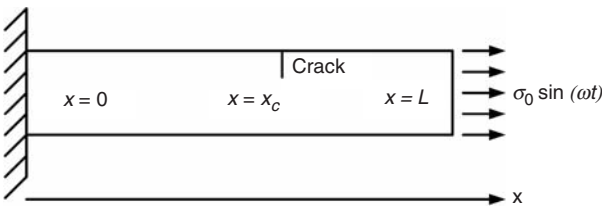

Figure 1 A schematic of a cracked beam with a harmonic excitation.

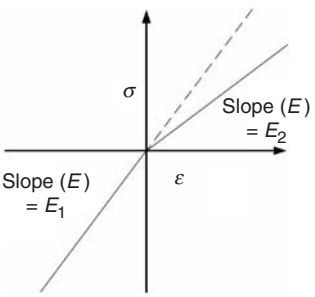

Figure 2 Bilinear stress–strain relation at the crack location ($x = x_c$).

and boundary condition:

$$\left.\left(E\frac{\partial u}{\partial x}\right)\right|_{x=L} = \sigma_0 \sin(\omega t) \tag{1c}$$

The damping coefficient in the elastic medium of the beam is assumed to be negligible.

A purely analytical solution of Equation (1) is difficult to obtain. Therefore, an approximate solution of the problem is sought through a variational formulation of Equation (1). At first, the displacement field is discretized in space as following:

$$\hat{u} = \sum_i g_i(t)\phi_i(x) \tag{2}$$

where $\phi_i(x)$ are the shape functions and $g_i(t)$ are the corresponding coefficients. $\hat{u}$ is an approximation for u. The weak form of Equation (1) is then formulated using the Galerkin technique (Equation (3)). Please note that the trial function, $\hat{u}$, and the test function, v, must satisfy the essential and homogeneous boundary conditions, respectively. Same basis functions are used for both $\hat{u}$ and v, as in the ordinary Galerkin method.

$$\int_{x=0}^{L}\left\{\rho\frac{\partial^2\hat{u}}{\partial t^2} - \frac{\partial}{\partial x}\left(E\frac{\partial\hat{u}}{\partial x}\right)\right\}v\,\mathrm{d}x + \left\{\left.\left(E\frac{\partial\hat{u}}{\partial x}\right)\right|_{x=L} - \sigma_0\sin(\omega t)\right\}v|_{x=L} = 0 \tag{3}$$

Equation (3) may be reduced to the well-known form of the equation of forced oscillation of a multi degrees of freedom system:

$$\mathbf{M}\frac{\partial^2\tilde{g}}{\partial t^2} + \mathbf{K}\tilde{g} = \tilde{f} \tag{4a}$$

where the superscript $\tilde{}$ is used to denote vectors. The matrices $\mathbf{M}$ and $\mathbf{K}$ are given by: $\mathbf{M}_{j,i} = \int_{x=0}^{L}\rho\phi_i\phi_j\,\mathrm{d}x$, and $\mathbf{K}_{j,i} = \int_{x=0}^{L}E\frac{\partial\phi_i}{\partial x}\frac{\partial\phi_j}{\partial x}\,\mathrm{d}x$, and the vector $\tilde{f}$ is given by $f_j = \sigma_0\sin(\omega t)\phi_j|_{x=L}$. $\mathbf{M}_{j,i}$ is the element in the jth row and ith column of $\mathbf{M}$. Similar definition goes for $\mathbf{K}$. f_j is the jth element of $\tilde{f}$. From Equation 4, the solution for

the vector $\tilde{g}$ is sought subject to the initial conditions:

$$\left.g_i\right|_{t=0} = 0 \quad \forall i$$
$$\left.\frac{\partial g_i}{\partial t}\right|_{t=0} = 0 \quad \forall i \tag{4b}$$

The above initial conditions follow from Equation (1b).

Equation (4) is otherwise a linear differential equation except that the matrix **K** changes between closed and open configurations of the crack. Since the excitation is harmonic with frequency ω, the steady state solution for $\tilde{g}$ is also harmonic with the same frequency. However, since the matrix **K** changes between the closed and open states of the crack, the amplitude of oscillation would be different between these two states. Let us assume that the solution for $\tilde{g}$ is $\tilde{g}_1 \sin(\omega t)$ when the crack is closed and $\tilde{g}_2 \sin(\omega t)$ when the crack is open. A strain gage affixed on the beam at $x = x_s$, say, therefore records a strain of $(\varepsilon_1|_{x=x_s}) \sin(\omega t)$ when the crack is closed and $(\varepsilon_2|_{x=x_s}) \sin(\omega t)$ when it is open. $\varepsilon_1|_{x=x_s}$ and $\varepsilon_2|_{x=x_s}$ are given by: $\varepsilon_1|_{x=x_s} = \sum_i \tilde{g}_{1_i} \frac{\partial \phi_i}{\partial x}\big|_{x=x_s}$ and $\varepsilon_2|_{x=x_s} = \sum_i \tilde{g}_{2_i} \frac{\partial \phi_i}{\partial x}\big|_{x=x_s}$. Since $\tilde{g}_1$ and $\tilde{g}_2$ are different, so are $\varepsilon_1|_{x=x_s}$ and $\varepsilon_2|_{x=x_s}$. Hereafter, it is shown using a numerical example that the amplitude spectrum of a nearly harmonic signal with two different amplitude contents (Equation (5)) would contain harmonics of the fundamental frequency (Figure 3). The amplitude spectrum is computed using Fast Fourier Transform (FFT). It can be observed from Figure 3 that a 1% change in amplitude results in visible even-harmonics in the frequency spectrum. Thus, it is shown in this section that a crack, modeled as a bilinear stiffness element in the structure, can cause production of certain super-harmonics when the structure is excited with a harmonic excitation.

$$y = \begin{cases} \sin(\omega t) & \text{if } y \geq 0 \\ 0.99 \sin(\omega t) & \text{if } y < 0 \end{cases} \tag{5}$$

where $\omega = 2\pi \times 250 \times 10^3$ Hz, and t is in seconds.

Although the bilinear stiffness model of a crack has been used in many studies [14,16–19,23] including the present one, the derivations presented above suggest that this model has certain limitations. First of all, the solution results in a sudden transition in the velocity field when the structure changes its configuration from open crack to closed crack and vice versa. This can be seen as a direct effect of the sharp transition of the local Young's modulus at the crack location when the crack opens or closes (Figure 2). Secondly, odd-harmonics are not observed through this formulation. Experimental results, however, show the presence of third harmonics in certain cases. Last, but not the least, a system with bilinear stiffness (and transition occurring at zero strain) is one of those rare kinds of nonlinear systems which display homogeneity [25]. As a result, the harmonic amplitudes are predicted by this model to vary linearly with the exciting amplitude. This linear variation is confirmed through numerical simulation by scaling y in Equation 5 with integers from 2 to 6, and the result is shown in Figure 4. On the contrary, experimental results confirm that the harmonic

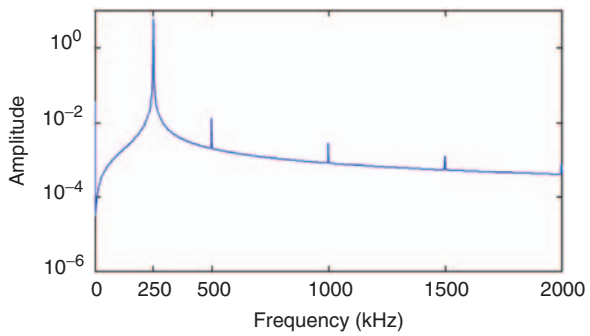

Figure 3 Amplitude spectrum of a nearly harmonic signal given by Equation 6.

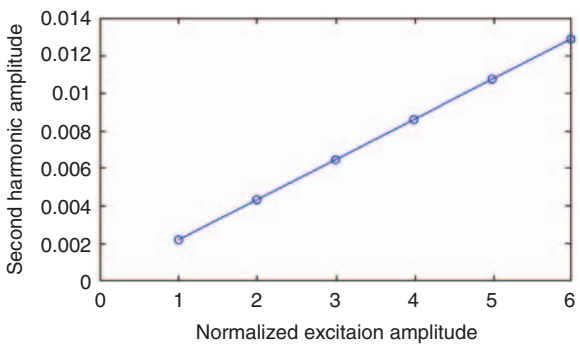

Figure 4 Linear variation of the second harmonic amplitude with excitation voltage.

amplitudes vary rather nonlinearly with exciting voltage.

The complexity of the interaction of acoustic waves with real defects is beyond the scope of current theoretical methods. However, some aspects of the wave-crack interaction can be explained, at least qualitatively, with a more detailed model of the crack *viz*. the Greenwood and Williamson's model [24,26]. Most importantly, the Greenwood and Williamson's model can explain the presence of odd-harmonics and the nonlinear variation of the harmonic amplitudes with exciting voltage.

The proposed technique identifies the presence of cracks in a structure by looking at the harmonics of the exciting frequency in the output signal and their nonlinear relationship to the input amplitude [24]. The amplitudes corresponding to the harmonics can be computed automatically using a FFT. It is worth mentioning here that harmonics of the driving frequency are expected to be present even in the output signal from an undamaged specimen because of unknown sources of nonlinearity; e.g., nonlinearity in the attached circuit. Therefore, it will be a challenging task to distinguish between nonlinearity produced by a crack and nonlinearity produced by other sources. However, from experimental results it appears that the amplitude of the harmonics due to unknown sources of nonlinearity and the degree of their variation with the excitation voltage are smaller compared to those due to crack-nonlinearity. Therefore, it is assumed in this study that this type of the excitation amplitude dependent nonlinearity is mainly attributed to crack formation. To detect cracks, results obtained from a cracked specimen must be compared with baseline results from the pristine condition of the same specimen. Larger amplitudes of harmonics and greater variation thereof with excitation voltage indicate crack(s) in the structure.

3 Experimental Results

The effectiveness of the proposed technique has been tested on an aluminum specimen and a steel specimen. The results are detailed in the following sections. To ensure that crack opening and closing happens at the fullest extent, the exciting frequency was always chosen to be the same as the resonant frequency of the transducer-structure system.

3.1 Experimental Results from Aluminum Specimen

The overall test configuration and the aluminum test specimen are shown in Figure 5. The specimen consisted of a rectangular cross-sectional beam 53.34 cm long, 7.14 cm wide, and 0.64 cm thick. The crack was made at the center of the beam-span and runs transversely across the width of the beam.

To produce the crack, a sharp notch was first made at the center of the beam. The beam was then subjected to cyclic loading under an INSTRON loading machine until a visible fatigue crack developed at the notch site. It took about 5000 cycles to produce a visible crack under 0.2 Hz cyclic loading a tensile stress range at the

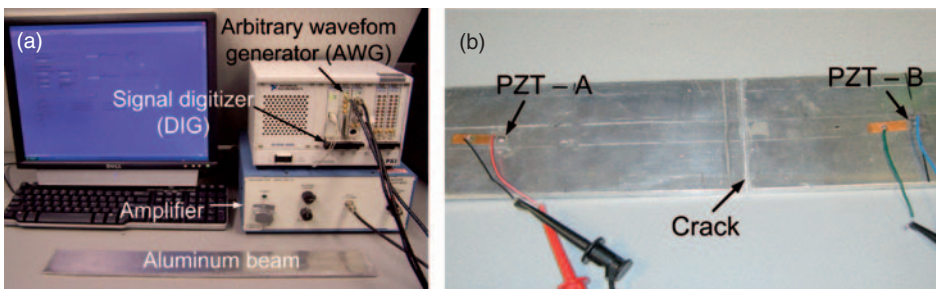

Figure 5 Experimental setup for detecting cracks on aluminum beam: (a) data acquisition system and the undamaged beam (b) Part of the beam showing the crack and the PZT transducers.

notch of 180 MPa. Two PSI-5A4E type PZT wafer transducers (1.0 cm × 1.0 cm × 0.0508 cm) were mounted on the beam so that the distance between them was 17.78 cm centered on the crack.

The data acquisition system was composed of an arbitrary waveform generator (AWG), a high-speed signal digitizer (DIG), and a linear amplifier. The gain of the amplifier was set to two. Using the 16-bit AWG, a Gaussian white noise signal with a 20 V peak-to-peak (p-p) voltage was generated and applied to one of the transducers (PZT-A in Figure 5). PZT-A generated elastic waves and the response was measured at PZT-B. When the waves arrived at PZT-B, the voltage output from PZT-B was measured by the DIG. The sampling rate and resolution of the DIG were 10 MHz and 14 bits, respectively. Thereafter, FFT of the response measured at PZT-B was done and the resonant frequency of the transducer-structure system was identified from the power spectrum. In order to improve the signal-to-noise ratio, the forwarding signals were measured 30 times and averaged in the frequency domain.

Figure 6 shows the amplitude spectrum of the output signal for the transducer-structure system when Gaussian white noise input was applied to the actuator. It can be observed from Figure 6 that the resonant frequency of the cracked system did not vary significantly from the resonant frequency of the undamaged system. Therefore, the driving frequency for all subsequent experiments for all undamaged, notched, and cracked states of the beam was chosen to be 250 kHz. Another resonant frequency was observed at 493 kHz (Figure 6). However, the response at 493 kHz was smaller compared to that at 250 kHz. Since the frequency resolution of the DIG was set to as low as 0.1 kHz, 493 kHz is not considered to be the second harmonic of 250 kHz.

Once the resonant frequency of the system was identified, a sinusoidal signal with a 2V p-p and driving frequency equal to the resonant frequency of the system was generated using the same AWG and applied to PZT-A. FFT of the response measured at PZT-B was taken, and the absolute values of the FFT at the second and third harmonics of the driving frequency were noted. Again, the forwarding signals were measured 20 times and averaged in the frequency domain. The above procedure was then repeated with the p-p excitation voltage varying from 2 V to 40 V with an incremental step of 2 V. The same experiment was repeated three times for each state of the specimen (i.e., undamaged, notched, and cracked) to see experiment to experiment variation. Note that the linearity of the amplifier used in this study is guaranteed only up to a certain output voltage, and this maximum voltage is determined from the maximum driving frequency (250 kHz) and the capacitance value of the transducer (4 nF) [27]. From the reference, it was found to be safe to apply up to 40V p-p without compromising the linearity of the amplifier.

Figure 7 shows that the first harmonic amplitude of the output signal varies more or

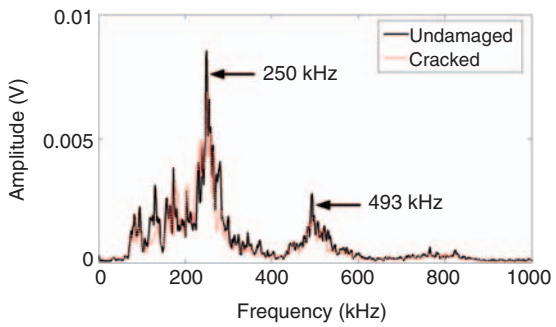

Figure 6 Amplitude spectrum of the output signal for Gaussian white noise input at 20 V p-p to the aluminum specimen.

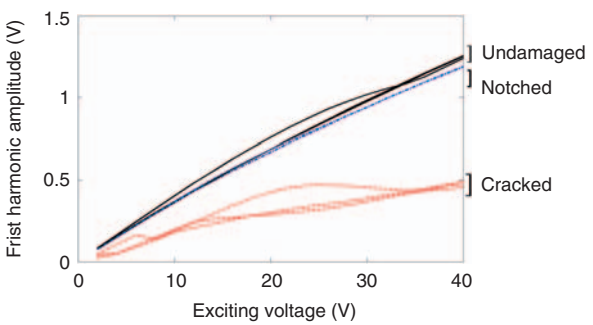

Figure 7 Variation of the first harmonic (250 kHz) amplitude in the output signal with excitation p-p voltage – results from three tests on the same aluminum specimen.

less *linearly* with the excitation voltage in the undamaged and notched cases as opposed to exhibiting *nonlinear variance* in the cracked case. This is an indication of nonlinearity due to crack, and the crack caused the energy corresponding to the driving frequency to be shifted among the higher harmonics. Additionally, the amplitude of the first harmonic is much lower in the cracked beam compared to its undamaged and notched counterparts. The above phenomenon can be attributed to reflection and scattering of acoustic waves from the crack interface. In addition, for the crack case, the amplitude of the first harmonic varies nonlinearly with increasing input voltage.

It can be observed from Figure 8 that beyond a certain value of the exciting voltage, the second, and third harmonic contents of the output signal are much more prominent in the cracked case than in the undamaged or notched cases. The variation of the harmonic amplitudes in the cracked specimen with increasing level of excitation is observed to be nonlinear. The presence of harmonics in the undamaged and notched states can be attributed to unknown sources of nonlinearity such as circuit-nonlinearity. The repeatability of the results shown in Figures 7 and 8 are acceptable in so far as the undamaged, notched, and cracked states of the beam can be easily classified.

In conclusion, it can be said that the cracked state of the aluminum beam could be distinguished from its undamaged and notched states by considering the amplitudes of the harmonic components and their variation with the excitation voltage.

3.2 Experimental Results from Steel Specimen

A second experiment was performed on a 2.74 m long W6 × 15 (SI: W150 × 22.5) steel beam. The dimensions of the steel specimen are shown in Figure 9(a). Two notches were cut into the bottom (tension) flange near the center of the beam-span as shown in Figure 9(b). These notches served as fatigue crack initiators, and also helped to increase the stress at this section in order to accelerate the development of fatigue cracks. The notches were designed to have a theoretical fatigue life on the order of 40,000 cycles at an applied stress range of 190 MPa. Notches on either side of the web were the same to mitigate any eccentric behavior. Fatigue cracks were expected to form at the sharp root of each notch.

Two PSI-5A4E type PZT wafer transducers (1.0 cm × 1.0 cm × 0.0508 cm) were mounted on the bottom flange of the beam so that the distance between them is 25 cm and the crack initiator falls between the transducers (Figure 10). Additionally, four electrical resistance crack gages were placed to monitor crack propagation. These were placed at the notch root on both sides of the flange (Figure 10(a)).

To produce the cracks, the beam was loaded in simple mid-span loading over a span length of 2.74 m. The midspan load was cycled from

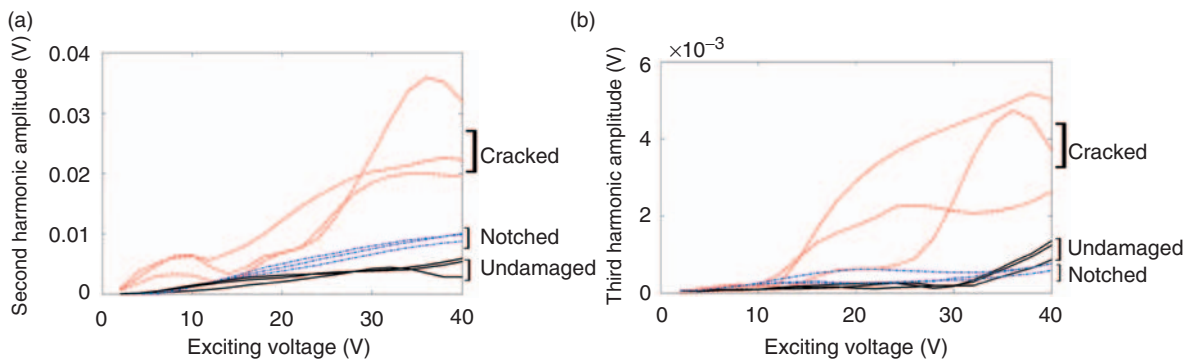

Figure 8 Variation of (a) second harmonic (500 kHz) and (b) third harmonic (750 kHz) amplitudes in the output signal with the increasing excitation voltage – results from three tests on the same aluminum specimen.

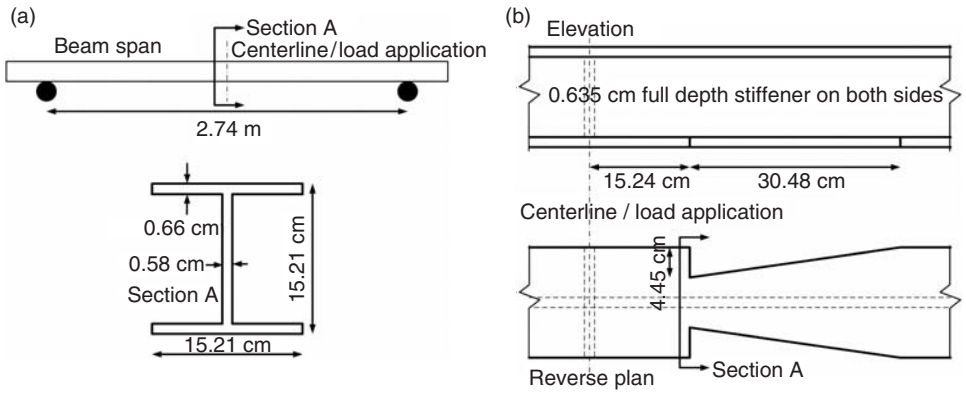

Figure 9 Dimensions of the steel W6 × 15 (SI: W150 × 22.5) section: (a) Beam span and cross section (b) Elevation and plan views of the flange in the tension side.

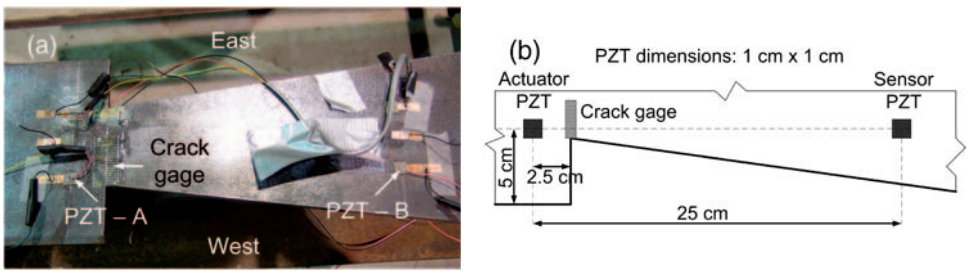

Figure 10 Part of the tension flange of the steel beam: (a) The notch, the PZT wafers and the crack gages (b) Schematic figure showing transducers and crack gage locations.

4.5 kN to 40.5 kN resulting in a load range of 36 kN. Cycling was carried out at a rate of 1 Hz. The 36 kN applied load corresponds to a tensile stress range of 190 MPa at the notch root of the tension flange. The minimum stress, at an applied load of 4.5 kN is 22.7 MPa. The loading set-up is shown in Figure 11. The notch site was continuously monitored for crack initiation. After 9000 cycles, cracks at each notch root were identified by the crack gages and could be observed visually. Figure 12 shows the crack on the Western side of the tension flange propagating beneath a crack gage after ~18,000 cycles. Figure 13 shows the history of crack propagation in the West flange of the steel beam.

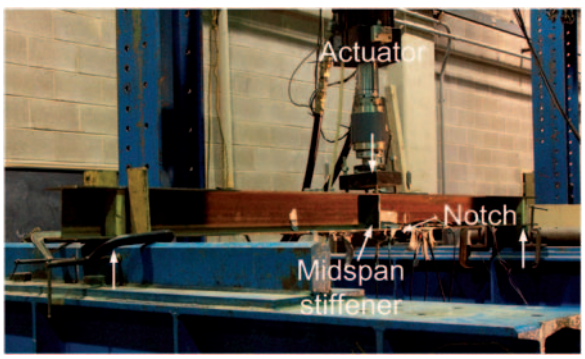

Figure 11 Loading configuration for the experiment on the steel beam.

Following every few thousand cycles (after 0, 5,000, 10,000, 12,000, 14,000, 18,000, 22,000, and 24,000 cycles to be precise), the cyclic loading was paused and a static load of 22 kN (average of fatigue load stress range) was applied to the beam. Under this constant load, data from the PZT transducers were collected following the same procedure that was performed on the aluminum beam. It should be mentioned that the resonant frequency of the transducer-structure system was measured once at the onset of loading and once after 12,000 cycles when the crack

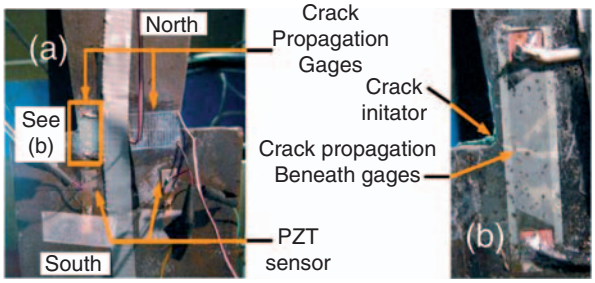

Figure 12 Part of the tension flange of the steel beam showing the location of the crack.

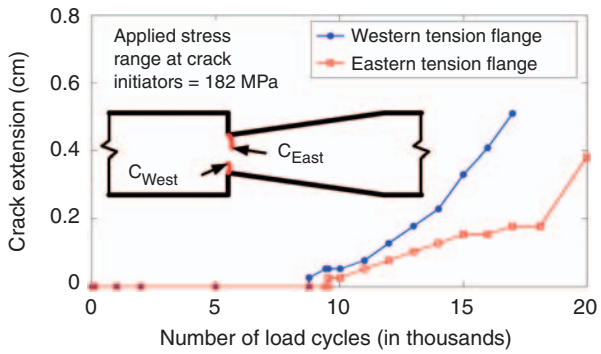

Figure 13 Propagation history of the crack emanating from the notch-tip of West part of the tension flange of the steel beam.

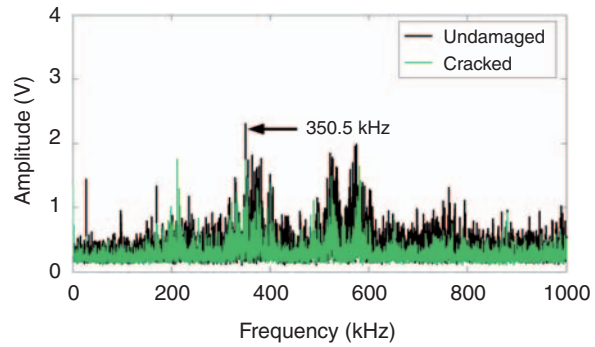

Figure 14 Amplitude spectrum of the output signal for Gaussian white noise input at 20V p-p to the steel specimen.

already existed (Figure 14). Figure 14 shows the amplitude spectrum of the output signal for the transducer-structure system when a Gaussian white noise input is given to the actuator. It can be observed from Figure 14 that the resonant frequency of the cracked system does not vary significantly from the resonant frequency of the undamaged system. The driving frequency for all subsequent experiments was therefore chosen to be 350.5 kHz, and the amplitude spectrum was not measured again due to time constraints. For a Gaussian white noise, the energy is distributed among so many frequencies that the second harmonic of a particular frequency (caused by the crack nonlinearity, which is usually small) is hardly discernable.

The results discussed in this section were obtained from the West side of the tension flange where collected data was more consistent. A fatigue crack also formed on the East side of the flange and was successfully captured by the crack gages. However, the PZT-based system failed to identify this crack before 20,000 cycles. This fact does not give the crack gages any edge over the PZT-based system because in practice the exact location of crack initiation will hardly be known in advance and the crack gages must traverse the crack (crack gages are conventionally applied following crack initiation to monitor crack propagation). The successful detection of a crack using PZT transducers depends upon a number of factors *viz*. nature of the crack, position of the PZT relative to the crack etc. It is difficult to specify which of the above factor(s) is (are) responsible for the successful detection of the crack on Western part of the flange and for the failure to detect crack on the Eastern part of the tension flange.

Figure 15(a) suggests an increased acoustic nonlinearity at ~10,000 cycles when the first harmonic amplitude varies nonlinearly with the excitation voltage. The presence of the second harmonic is also significant around ten thousand cycles (Figure 15(b)). These observations combined with observations from the crack gages (Figure 13) imply that the PZT-based active sensing system could identify the damage near its inception.

Figure 16 shows the variation of the first and second harmonic amplitudes in the output signal with the increasing number of loading cycles for an excitation voltage of 40V p-p. In Figure 16, the first harmonic amplitude shows a general downward trend which can be attributed to

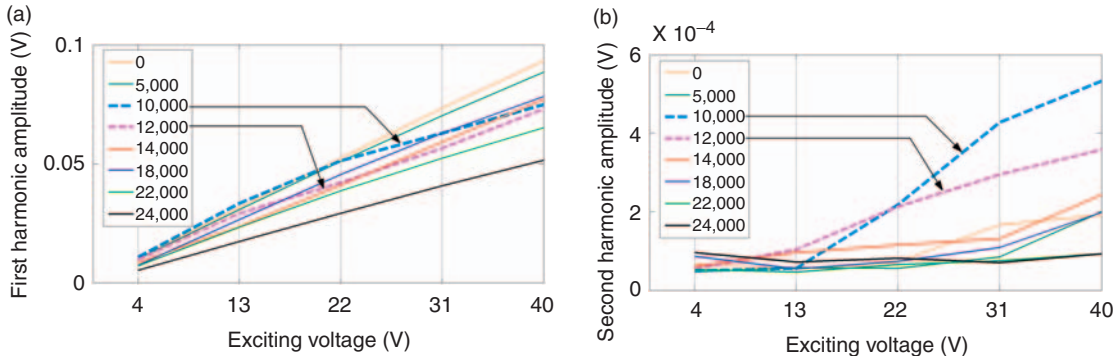

Figure 15 Variation of (a) first harmonic (350.5 kHz) and (b) second harmonic amplitudes (701 kHz) in the output signal with the increasing excitation p-p voltage after given number of cycles of loading; Crack initiated around 8790 cycles.

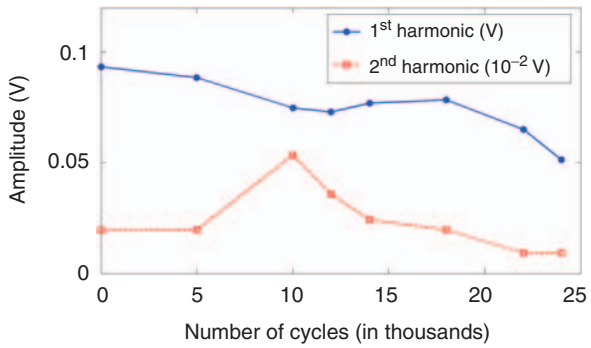

Figure 16 Variation of first (350.5 kHz) and second harmonic (701 kHz) amplitudes in the output signal with respect to the number of loading cycles for an excitation voltage of 40V p-p.

reflection and scattering of acoustic waves from the crack interface. However, around 10,000 cycles, the first harmonic amplitude dips unusually, which may be explained by energy shifting to the higher harmonics. The same figure also shows the trend of the second harmonic amplitude which is unusually high around 10,000 cycles. The following may therefore be inferred from the above observations: the nonlinearity effects became prominent at the inception of the crack, but its manifestation decreased steadily with increasing length of the crack and became indiscernible after 14,000 cycles. There are two possible explanations for this observed phenomenon. First, the crack tip gets wider as crack propagates, and crack opening and closing becomes insignificant. Secondly, the crack tip moves away from the line of sight of the PZT actuator-sensor couple. This results in oblique incidence of the acoustic waves on the crack tip, which is not strong enough to produce crack opening and closing. Whatever the reason, this observation suggests a highly localized nature of the sensing technique described in this study.

In conclusion, it can be said that the crack in the West part of the bottom flange of the steel beam could be identified at its inception by looking at the amplitudes of the harmonic component and their nonlinear variation with excitation voltage.

4 Conclusion

The objective of this study was to propose an easily automated crack detection technique in metallic structures using agile PZT transducers. Preeminent harmonics in the response signal from cracked specimens were observed as the input power of the driving PZT-wafer increased. The harmonic amplitudes also showed nonlinear variation with the increasing excitation voltage in cracked specimens. The proposed technique identifies the presence of cracks by looking at two features: harmonics and their nonlinear relationship to the input amplitude. Although the essence of crack detection remains the same for both the specimens, the effect of nonlinearity is far less pronounced in the case of the steel beam (e.g., compare Figures 8(a) and 15(b)). Since the size and stiffness of the steel specimen are greater than those of the aluminum plate, the amplitude of vibration in steel is smaller compared to that in

aluminum for the same level of excitation voltage. Because of the low amplitude of oscillation, the extent of crack opening and closing is reduced and hence nonlinear wave interaction does not take place at a measurable level for the steel specimen. Experimental results also showed the presence of second and third-order harmonics in the undamaged and notched states of a structure caused by unknown sources of nonlinearity. Further study is warranted to address the issue of distinguishing the nonlinearity due to cracks from nonlinearity due to unknown sources. Nevertheless, it is possible to identify cracks in a specimen by looking at the greater magnitude of the harmonics and higher amount of their variation with the excitation voltage as compared to those in the pristine state of the structure. Another interesting study would be to investigate the effectiveness of this technique by varying the position to the PZTs relative to the crack. At this point, it can be said that the two main concerns are: (1) the distance of an actuator or a sensor from the crack, and (2) the orientation of the crack relative to the line of sight between the actuator and the sensor. Since guided waves are known to propagate large distances without much attenuation, it is envisioned that the effectiveness of the proposed technique would not be significantly affected by the relative location of the crack and the PZTs. This claim, however, needs to be corroborated by experimental data and relevant work in this direction is considered a part of the authors' future work.

Acknowledgments

This research is supported by the Radiation Technology Program under Korea Science and Engineering Foundation (KOSEF) and the Ministry of Science and Technology (M20703000015-07N0300-01510) and Korea Research Foundation (D00462).

References

1. Huang, M., Jiang, L., Liaw, P.K., Brooks, C.R., Seeley, R. and Klarstrom, D.L. (1998). Using acoustic emission in fatigue and fracture materials research. *JOM-e*, *50*(*11*), http://www.tms.org/pubs/journals/JOM/9811/Huang/Huang-9811.html
2. Sophian, A., Tian, G.Y., Taylor, D. and Rudlin, J. (2001). Electromagnetic and eddy current NDT: a review. *Insight* (*UK*), *43*(*5*), 302–306.
3. Chondros, T.G., Dimarogonas, A.D. and Yao, J. (1998). A continuous cracked beam vibration theory. *Journal of Sound and Vibration*, *215*(*1*), 17–34.
4. Liang, C., Sun, F.P. and Rogers, C.A. (1994). Coupled electro-mechanical analysis of adaptive material systems – determination of the actuator power consumption and system energy transfer. *Journal of Intelligent Material Systems and Structures*, *5*, 12–20.
5. Giurgiutiu, V. and Rogers, C.A. (1997). Electro-mechanical (E/M) impedance method for structural health monitoring and non-destructive evaluation. *International Workshop on Structural Health Monitoring*, Stanford. CA, USA, pp. 433–444.
6. Park, G., Sohn, H., Farrar, C.R. and Inman, D.J. (2003). Overview of piezoelectric impedance-based health monitoring and path forward. *The Shock and Vibration Digest*, *35*(*6*), 451–463.
7. Green, R.E. (1973). *Ultrasonic Investigation of Mechanical Properties*, New York and London: Academic Press.
8. Rose, J.L. (1999). *Ultrasonic Waves in Solid Media*, UK: Cambridge University Press.
9. Kim, S.B. and Sohn, H. (2007). Instantaneous reference-free crack detection based on polarization characteristics of piezoelectric materials. *Smart Materials and Structures*, *16*(*6*), 2375–2387(13).
10. Staszewski, J.W. (2003). Structural health monitoring using guided ultrasonic waves. In: Holnicki-Szulc, J. and Mota Soares, C.A. (eds), *Advances in Smart Technologies in Structural Engineering*, pp. 117–162.
11. Rizzo, P. and Lanza di Scalea, F. (2007). Wavelet-based unsupervised and supervised learning algorithms for ultrasonic structural monitoring of waveguides. In: Reece, P.L. (ed.), *Progress in Smart Materials and Structures Research*, Ch. 8, pp. 227–290, NOVA science publishers Inc., New York.
12. Kundu, T. (2004). *Ultrasonic Nondestructive Evaluation: Engineering and Biological Material*, CRC Press, Florida, ISBN 0849314623.
13. Buck, O., Morris, W.L. and Richardson, J.M. (1978). Acoustic harmonic generation at unbonded interfaces and fatigue cracks. *Appl. Phys. Lett.*, *33*(*5*), 371–373.
14. Richardson, M. (1979). Harmonic generation at an unbonded interface. I. Planar interface between semi-infinite elastic media. *Int. J. Eng. Sci.*, *17*, 73–75.
15. Morris, W.L., Buck, O. and Inman, R.V. (1979). Acoustic harmonic generation due to fatigue damage in high-strength aluminum. *J. Appl. Phys.*, *50*(*11*), 6737–6741.

16. Kawashima, K., Omote, R., Ito, T., Fujita, H. and Shima, T. (2002). Nonlinear acoustic response through minute surface cracks: FEM simulation and experimentation. *Ultrasonics*, *40*(*1–8*), 611–615.
17. Kogl, M., Hurlebaus, S. and Gaul, L. (2004). Finite element simulation of non-destructive damage detection with higher harmonics. *NDT & E International*, *37*(*3*), 195–205.
18. Hillis, A.J., Neild, S.A., Drinkwater, B.W. and Wilcox, P.D. (2006). Global crack detection using bispectral analysis. *Proceedings of the Royal Society A*, *462*, 1515–1530.
19. Rivola, A. and White, P.R. (1998). Bispectral analysis of the biharmonic oscillator with application to the detection of fatigue cracks. *Journal of Sound and Vibration*, *216*(*5*), 889–910.
20. Donskoy, D.M. and Sutin, A.M. (1998). Vibro-acoustic modulation nondestructive evaluation technique. *Journal of Intelligent Material Systems and Structures*, *9*, 765–771.
21. Parsons, Z. and Staszewski, W.J. (2006). Nonlinear acoustics with low-profile piezoceramic excitation for crack detection in metallic structures. *Smart Materials and Structures*, *15*, 1110–1118.
22. Lee, Y.L., Pan, J., Hathaway, R. and Barkey, M. (2005). Fatigue damage theories, *Fatigue Testing and Analysis*, 57, Elsevier Inc., Boston.
23. Friswell, M.I. and Penny, J.E.T. (2002). Crack modeling for structural health monitoring. *Structural Health Monitoring*, *1*(*2*), 139–148.
24. Pecorari, C. (2003). Nonlinear interaction of plane ultrasonic waves with an interface between rough surfaces in contact. *J. Acoust. Soc. Am.*, *113*(*6*), 3065–3072.
25. Worden, K. and Tomlinson, G.R. (2001). *Nonlinearity in Structural Dynamics*, p. 49, and 55, Institute of Physics Publishing, Bristol and Philadelphia.
26. Greenwood, A. and Williamson, J.B.P. (1966). Contact of nominally flat surfaces. *Proc. R. Soc. London, Ser. A*, *295*, 300–319.
27. http://www.piezo.com/prodelect1epa104.html

SHM
Structural Health Monitoring

Errata

Erratum (DOI of erratum: 10.1177/1475921709107051)

Debaditya Dutta, Hoon Sohn, Kent A. Harries and Piervincenzo Rizzo. A Nonlinear Acoustic Technique for Crack Detection in Metallic Structures. Structural Health Monitoring: An International Journal, first published on March 13, 2009 as 10.1177/1475921708102105. This version is no longer available. The version of record is published in Vol 8 No 3, as 10.1177/1475921709102105.

Erratum (DOI of erratum: 10.1177/1475921709107052)

Haitao Zheng and Akira Mita. Localized Damage Detection of Structures Subject to Multiple Ambient Excitations Using Two Distance Measures for Autoregressive Models. Structural Health Monitoring: An International Journal, first published on March 6, 2009 as 10.1177/1475921709102145. This version is no longer available. The version of record is published in Vol 8 No 3 as 10.1177/1475921708102145.

Erratum (DOI of erratum: 10.1177/1475921709107053)

Zhongqing Su, Xiaoming Wang, Li Cheng, Yu Long, and Zhiping Chen. On Selection of Data Fusion Schemes for Structural Damage Evaluation. Structural Health Monitoring: An International Journal, first published on March 6, 2009 as 10.1177/1475921709102140. This version is no longer available. The version of record is published in Vol 8 No 3 as 10.1177/1475921708102140.

Erratum (DOI of erratum: 10.1177/1475921709107054)

Xianhua Liu. Robust Damage Metric in terms of Magnitude and Phase for Impedance Based Structural Health Monitoring. Structural Health Monitoring: An International Journal, first published on July 1, 2009 as 10.1177/1475921708102144. This version is no longer available. The version of record is published in Vol 8 No 4 as 10.1177/1475921709102144.

Erratum (DOI of erratum: 10.1177/1475921709107055)

Alessio Medda. Near-Field Sub-band Beamforming for Damage Detection in Bridges. Structural Health Monitoring: An International Journal, first published on June 30, 2009 as 10.1177/1475921708102169. This version is no longer available. The version of record is published in Vol 8 No 4 as 10.1177/1475921709102169.

Vol 8(6): 0573–2
[1475-9217 (200911) 8:6;573–2 10.1177/1475921709349138]